Acoustic nonlinear imaging and its application in tissue characterization*

Dong Zhang and Xiu-fen Gong

Lab. of Modern Acoustics, Institute of Acoustics, Nanjing University,

Nanjing 210093, China

ABSTRACT

Acoustic nonlinear imaging has brought about significant improvements in image quality by taking advantage of the nonlinear components. This paper reviews works on acoustic nonlinear imaging for biological tissues in our Laboratory, including acoustic nonlinearity parameter B/A imaging, tissue harmonic imaging by using the multi-phase-coded-pulse technique and super harmonic imaging. Theoretical analysis and experimental imaging of biological tissues by using these methods are presented.

1. INTRODUCTION

Ultrasound imaging has been widely accepted for clinical diagnosis because of its capability to provide important information on the diseased state of the tissues in a human body non-invasively and non-destructively. In recent years, ultrasound image quality has been greatly improved due to advances in technology and introduction of new techniques, such as tissue harmonic imaging [1-3]. The acoustic nonlinear effects in biological tissues at biomedical frequencies and intensities were first theoretically predicted and experimentally demonstrated [4-5]. The second and higher harmonic components are generated as ultrasound propagates through biological tissues due to the phenomenon of nonlinear sound propagation. Tissue harmonic imaging uses ultrasound at twice the transmitted frequency to form the image, unlike the fundamental imaging that uses ultrasound at the transmitted frequency to form the image. Although it is superior to fundamental imaging mode due to improvement of the spatial resolution and suppression of side lobe levels, two typical shortcomings are associated with this technique. One is that the low signal-to-noise ratio (SNR) limits the penetration depth in ultrasonic diagnosis due to the much lower energy at the second harmonic frequency than that at the fundamental

* Supported by the Natural Science Foundation of China (No: 10474040)

frequency. Another is related with the narrow bandwidth signals in the transmitting system for reducing the side-lobe levels and the harmonic leakage, which results in degraded axial resolution. Much attention has been focused on the study of the nonlinear effect in biological tissues [6-13], and on the development of the acoustic nonlinear imaging techniques [14-24].

In this paper, works on acoustic nonlinear imaging in our Lab are reviewed. (1) As a measure of the nonlinearity in the pressure-density relation for a medium, the nonlinearity parameter B/A plays a significant role in nonlinear acoustics [25], and has been found some dependence on the compositions and structure features of biological tissues [26-27]. Thereby this parameter has been proposed to be a new parameter for tissue characterization, and could have some potential applications in ultrasonic diagnosis. We present here the B/A imaging via the measurement of second harmonics. (2) We present a multiple-phase-coded-pulse technique to provide the desired enhancement of SNR for high order harmonic ultrasonic imaging. In this technique, N phase-coded pulses are transmitted in sequence, the N^{th} order harmonic component in the echo signal is extracted with a gain of $20\log_{10} N$ dB compared with that in the single pulse harmonic imaging mode, whereas the fundamental and other order harmonic components are efficiently suppressed to reduce image confusion. Consequently, SNR is increased by $10\log_{10} N$ dB. (3) A super-harmonic component is defined as a summation of the third-, fourth- and fifth-order harmonic components [28]. We study the super-harmonic generation and imaging in biological tissues.

2. NONLINEARITY PARAMETER B/A IMAGING

B/A arise from the Taylor series expansion expressing the variations in pressure with density in a medium. It is defined by the ratio of the quadratic to linear terms in the Taylor series [25],

$$\frac{B}{A} = 2\rho_0 c_0 \left(\frac{\partial c}{\partial p}\right)_{s,0}, \qquad (1)$$

Basing on the finite amplitude theory, we have investigated the transmission B/A tomography via the second harmonics, the parametric array, as well as B/A tomography in reflection mode [20-22]. Here, the B/A imaging via the measurement of the second

harmonics is reviewed.

When a sample is inserted into the reference medium (water) between the transmitter and the receiver, the sound pressure amplitude for the second harmonics at distance L is:

$$p_{2x}(L) = \frac{\omega}{2} p_0^2 \int_0^L \beta_i(x) \exp[\int_0^x -2\alpha_1(x)dx - \int_x^L \alpha_2(x)dx]dx, \quad (2)$$

where p_0 is the source amplitude of sound pressure, $\beta_i(x)=\beta(x)/[\rho(x)c^3(x)]$, $\beta(x) = 1+\frac{1}{2}(\frac{B}{A})(x)$. $\alpha_1(x)$, $\alpha_2(x)$ are sound attenuation coefficients for fundamental and second harmonic waves. When the sample is absent, we have

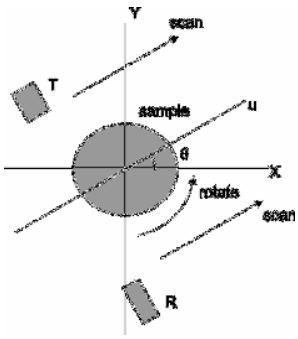

Fig. 1. The conventional CT scanning technique.

$$p_{20}(L) = \frac{\omega L}{2} p_0^2 \beta_{i0}, \quad (3)$$

where β_{i0} is the value of β_i for water. Using Eqs. (2) and (3), we obtain

$$\frac{p_{2x}(L)}{p_{20}(L)} = \frac{1}{\beta_{i0}L} \int_0^L \beta_i(x) \exp[\int_0^x -2\alpha_1(x)dx - \int_x^L \alpha_2(x)dx]dx. \quad (5)$$

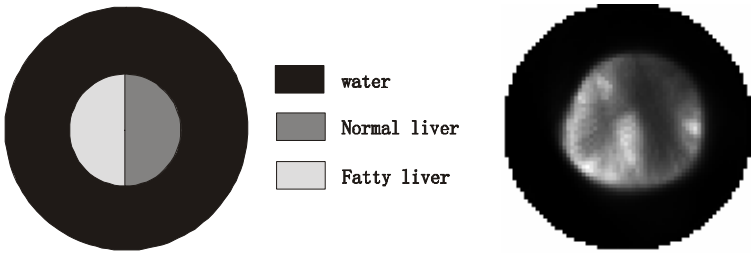

Fig. 2. (a) Cross section of sample model, (b) B/A image of the sample.

By considering $p_{2x}(L)/p_{20}(L)$ as projection data $P(u,\theta)$ in a conventional CT scanning technique (Fig. 1), we reconstruct the tomography of $\beta_i(x,y)$ corrected by an attenuation matrix $C(x,y)$ defined by

$$C(x,y) = \frac{1}{2\pi} \int_0^{2\pi} \exp[\int_{-V_1}^{v} -2\alpha_1(x,y)dv - \int_v^{V_1} \alpha_2(x,y)dv]d\theta, \quad (5)$$

where $V_1=L/2$. Figure 2 shows a B/A tomography for a sample combined with normal porcine liver and a kind of pathological porcine liver (fatty liver). From the result, we find that the value of B/A for the fatty liver increases, and the corresponding part in the image exhibits higher gray.

3. MULTI-PHASE-CODED-PULSE TECHNIQUE

A burst signal with angular frequency ω and initial phase φ_0 is radiated in a

medium, and the sound pressure at distance $x = 0$ is $p_0 \sin(\omega t + \varphi_0)$. From the Fubini series solution of the Burgers' equation [25], the sound pressure at distance x is:

$$p(x) = \sum_{m=1}^{\infty} \frac{2p_0}{m\sigma} J_m(m\sigma) \sin(m\omega\tau + m\varphi_0), \qquad (6)$$

where m is the order of the harmonics. $\sigma = x / x_k$ is the axial normalized distance, $x_k = (\beta M k)^{-1}$ is the distance of shock formation, $k = \omega / c_0$ is the wave number, β is the nonlinearity coefficient, $M = v_0 / c_0$ is the acoustic Mach number, where v_0 and c_0 are the particle velocity and isentropic sound speed. t is the transmitting time and $\tau = t - x / c_0$ is the retarded time.

Suppose that N pulse signals with an equidistant phase φ_n are used to excite the transducer in sequence. If the initial phase of the first pulse signal is φ_0, the phase of the n th pulse signal is set to be $\varphi_n = \varphi_0 + 2\pi n / N$, where $n = 0,1,\ldots,N-1$. The sound pressure of the n th transmitted pulse signal at the source is expressed as

$$p_n(0) = p_0 \sin(\omega t + \varphi_n) = p_0 \sin(\omega t + \varphi_0 + 2\pi n / N) \qquad n = 0 \text{ to } N-1. \qquad (7)$$

According to Eqs. (6) and (7), the sound pressure at distance x for the n^{th} transmitted pulse signal is:

$$p_n(x) = \sum_{m=1}^{\infty} \frac{2p_0}{m\sigma} J_m(m\sigma) \sin[m\omega\tau + m(\varphi_0 + 2\pi n / N)] \ . \qquad (8)$$

The summation of the received signals of the N phase-coded transmitted signals at distance x is:

$$p_s(x) = \sum_{n=0}^{N-1} \sum_{m=1}^{\infty} \frac{2p_0}{m\sigma} J_m(m\sigma) \sin[m\omega\tau + m(\varphi_0 + 2\pi n / N)]. \qquad (9)$$

From Eq. (9), we can find that the sound pressure of the m th order harmonic component in the summation is:

$$p_{sm}(x)=\sum_{n=1}^{N-1}\frac{2p_0}{m\sigma}J_m(m\sigma)\sin[m\omega\tau+m(\varphi_0+2\pi n/N)]. \qquad (10)$$

From Eq. (10), the sound pressure of the summation is:

$$p_{sm}(x)=\begin{cases}\dfrac{2p_0}{m\sigma}J_m(m\sigma)\sum\limits_{n=1}^{N-1}\sin[m\omega\tau+m(\varphi_0+2\pi n/N)]=0 & m\neq N\\ N\dfrac{2p_0}{m\sigma}J_m(m\sigma)\sin(m\omega\tau+m\varphi_0) & m=N\end{cases}. \qquad (11)$$

By comparison of Eq. (11) with Eq. (6), the sound pressure of the N th order harmonic component using N phase-coded pulses is N times that of the single pulse. Meanwhile, the other harmonic components including the fundamental frequency are fully eliminated. In addition, the kN th (k is integer) order harmonics also can be increased by N times. The phase inversion technique is the special case of N =2 (Ma et al 2005). It is concluded that the selected harmonic component can be efficiently extracted with harmonic enhancement of $20\log_{10}N$ dB in high order harmonic imaging by the use of N phase-coded pulses, and SNR still can be improved by $10\log_{10}N$ dB considering the noise energy incorporation.

In this paper, the second and higher harmonic imaging with multiple phase-coded pulses are carried out for biological tissues. As shown in Fig. 3, the sample is a piece of porcine fatty tissue with two holes (diameter 3 mm and 2 mm). In the reconstructed images in Fig. 4, the different gray scale corresponds to different biological tissues due to the difference in the amplitudes of the harmonic components. By means of multiple phase-coded pulses (N =2, 3, 4 and 5 respectively), the processed acoustic

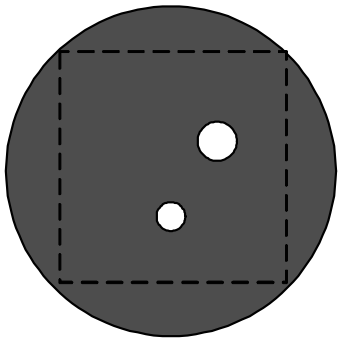

Fig. 3. Sample model

nonlinear images at the second to fifth order harmonic frequencies are presented in Fig. 4(b) to 4(e). For comparison, the fundamental frequency images are also given in Fig. 4(a). The two holes in Fig. 4(a) are vague and the shapes are not clearly displayed. In addition, there are lots of speckle noises in the fatty tissue for the ultrasound diffraction and side lobe level of the fundamental frequency. By means of the phase-coded pulse technique, the amplitudes of the processed high order harmonics are enhanced, which yield the improved brightness and contrast of the images as shown in Fig. 4(b) to 4(e). Along with the increase of the harmonic order, the resolution and the clarity of the images become better.

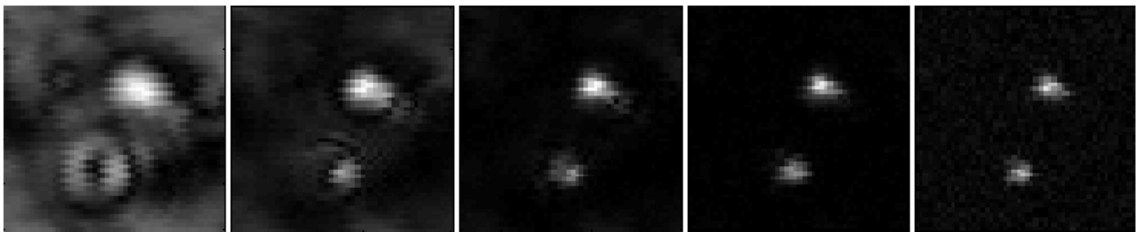

(a) (b) (c) (d) (e)

Fig. 4. Reconstructed images of sample model by the multi-phase-coded-pulse technique: (a) Fundamental Imaging, (b) 2th harmonic image, (c) 3rd harmonic image, (d) 4th harmonic image and (e) 5th harmonic image.

4. SUPER HARMONIC IMAGING

When a finite amplitude wave propagates in a medium, the nonlinear effects occur and the second and the higher harmonics are generated. The super-harmonic component is obtained by the linear summation of the absolute amplitudes of 3rd, 4th and 5th harmonics [28]. Fig. 5 shows a three-layer model B with a porcine fatty tissue located at both the external ring and the internal circle, and a porcine liver tissue located at the middle ring. The

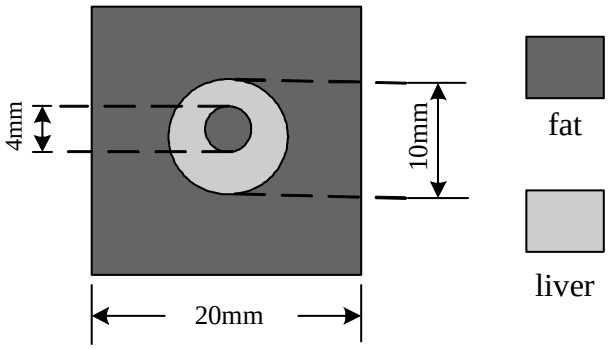

Fig. 5. Sample model.

corresponding fundamental, second harmonic and super-harmonic images are presented in Fig. 6, in which different gray scales correspond to different biological tissues due to the differences in the amplitudes of selected component of the received signal. Because the beam pattern at the super-harmonic frequency is improved (–3 dB beam width at the fundamental frequency is 1.3 times greater than that at the second order harmonic component and 1.7 times greater than that at the super-harmonic frequency), the super-harmonic image exhibits better spatial resolution than the fundamental or the second harmonic images. In the fundamental frequency image Fig. 6(a), it is observed that the edges of different tissues are vague and there exists an intergradation of about 2 mm from the poor spatial resolution at the fundamental frequency. With an improvement in spatial resolution, the second harmonic images demonstrate recognizable tissue combinations as shown in Fig. 6(b). The edges of the liver and fatty tissues are confirmed, but the lower amplitude of the second harmonic results in less contrast of the image. In the super-harmonic image as shown in Fig. 6(c), both the dimensions and positions of tissues are confirmed by the sharp borders and the contrast of the images is improved. In addition, the speckle noise in the fatty tissue is reduced.

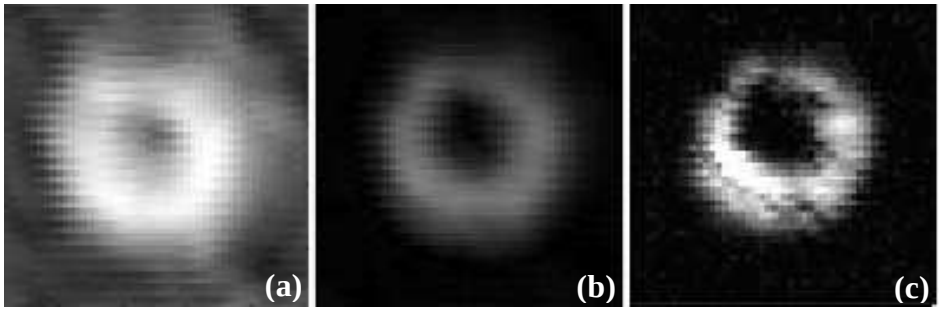

Fig. 6. Images of sample model: (a) Fundamental Imaging, (b) 2th harmonic image, (c) super-harmonic image.

5. CONCLUSION

This paper reviewed some researches on the acoustic nonlinear imaging in our laboratory. Further assessment of those techniques in clinical application is needed.

REFERENCES

[1] T. Christopher, IEEE UFFC, 44(1997), 125.

[2] C. C. Shen and P. C. Li, IEEE UFFC, 48(2001), 728.

[3] P. Jiang, Z. Mao, J. C. Lazenby, IEEE Ultrasonics Symposium, (1998)1589.

[4] T. G. Muir, E. L. Carstensen, ***Ultrasound in Med. & Biol.*** 6 (1980) 347.

[5] E. L. Carstensen, W. Law, N. D. Mckay, T. G. Muir, ***Ultrasound in Med. & Biol.*** 6 (1980) 359.

[6] W. K. Law, L. A. Frizzell, F. Dunn, ***Ultrasound in Med. & Biol.*** 11 (1985) 307.

[7] W. N. Cobb, ***J. Acoust. Soc. Am.*** 73 (1983) 1525.

[8] X. F. Gong, R. Feng, Z. Y. Zhu, ***J. Acoust. Soc. Am.*** 76 (1984) 949.

[9] C. M. Sehgal, R. C. Bahn, J. F. Greenleaf, ***J. Acoust. Soc. Am.*** 76 (1984) 1023.

[10] X. F. Gong, Z. M. Zhu, T. Shi, J. H. Huang, ***J. Acoust. Soc. Am.*** 86 (1989) 1.

[11] W. K. Law, L. A. Frizzell, F. Dunn, ***J. Acoust. Soc. Am.*** 69 (1981) 1210.

[12] J. Zhang, F. Dunn, ***J. Acoust. Soc. Am.*** 89 (1991) 80.

[13] J. Zhang, M. S. Kuhlenschmidt, F. Dunn, ***J. Acoust. Soc. Am.*** 89 (1991) 80.

[14] K. Yoshizumi, T. Sato, N. Ichida, ***J. Acoust. Soc. Am.*** 82 (1987) 302.

[15] N. Ichida, T. Sato, M. Linzer, ***Ultrasonic Imaging*** 9 (1983) 295.

[16] N. Ichida, S. Takuso, H. Miwa, K. Murakami, ***IEEE trans. Son. Ultrason***. SU-31 (1984) 635.

[17] C. A. Cain, ***J. Acoust. Soc. Am.*** 80 (1986) 28.

[18] F. Tranquart, N. Grenier, V. Eder, and L. Pourcelot, Ultrasound in Med. & Biol., 6(1999), 889.

[19] S. Tanaka, O. Oshikawa, T. Sasaki, T. Ioka, and H. Tsukuma, Ultrasound in Med. & Biol., 26(2000), 183.

[20] D. Zhang, X. F. Gong, S. G. Ye, ***J. Acoust. Soc. Am.*** 99 (1996) 2397.

[21] D. Zhang, X. F. Gong, ***Ultrasound in Med. & Biol.*** 25 (1999) 593.

[22] D. Zhang, X. Chen, X. F. Gong, ***J. Acoust. Soc. Am.*** 109 (2001) 1219.

[23] Q. Y. Ma, D. Zhang, X. F. Gong, Y. Ma, J. Acoust. Soc. Am. 119(2006) 2518.

[24] Q. Y. Ma, Y. Ma, X. F. Gong, D. Zhang, Ultrasound in Med. & Biol. 31(2005) 889.

[25] R. T. Beyer, ***J. Acoust. Soc. Am.*** 32 (1960) 719.

[26] R. L. Errabolu, C. M. Sehgal, R. C. Bahn, J. F. Greenleaf, ***Ultrasound in Med. & Biol.*** 14 (1988) 137.

[27] C. M. Sehgal, G. M. Brown, R. C. Bahn, J. F. Greenleaf, ***Ultrasound in Med. & Biol.*** 12 (1986) 865.

[28] A. Bouakaz, N. de Jong, IEEE UFFC, 44(2003), 125.